A hybrid, non-split, stiff/RKC, solver for advection-diffusion-reaction equations and its application to low-Mach number combustion

M. Lucchesi[a], H. H. Alzahrani[a], C. Safta[b], O. M. Knio[a]

[a]King Abdullah University of Science and Technology, Thuwal, Saudi Arabia
[b]Sandia National Laboratories, Livermore, CA, United States

ARTICLE HISTORY
Compiled February 13, 2019

ABSTRACT
We present a new strategy to couple, in a non-split fashion, stiff integration schemes with explicit, extended-stability predictor-corrector methods. The approach is illustrated through the construction of a mixed scheme incorporating a stabilized second-order, Runge-Kutta-Chebyshev method and the CVODE stiff solver. The scheme is first applied to an idealized stiff reaction-diffusion problem that admits an analytical solution. Analysis of the computations reveals that as expected the scheme exhibits a second-order in time convergence, and that, compared to an operator-split construction, time integration errors are substantially reduced. The non-split scheme is then applied to model the transient evolution of a freely-propagating, 1D methane-air flame. A low-mach-number, detailed kinetics, combustion model, discretized in space using fourth-order differences, is used for this purpose. To assess the performance of the scheme, self-convergence tests are conducted, and the results are contrasted with computations performed using a Strang-split construction. Whereas both the split and non-split approaches exhibit second-order in time behavior, it is seen that for the same value of the time step, the non-split approach exhibits significantly smaller time integration errors. On the other hand, the results also indicate that the application of the present non-split construction becomes attractive when large integration steps are used, due to numerical overhead.

KEYWORDS
stiff integrator; extended stability method; splitting errors; low-Mach-number combustion; direct numerical simulation

1. Introduction

Chemically-reacting flows are generally characterized by a large range of time scales, which typically leads to a stiff system of governing equations. Stiffness challenges specifically arise due to incorporation of detailed kinetic models, including a large number of elementary reactions evolving at disparate time scales. They also arise when resolved representations of thin reaction zone structures are achieved, which also leads to a broad range of diffusion time scales. Numerous efforts have consequently been dedicated to addressing these challenges, e.g. [1–14].

A well-established means of addressing the chemical stiffness of the governing equations in a homogeneous (0D) setting is based on the use of a fully implicit method [1–4].

CONTACT M. Lucchesi. Email: marco.lucchesi@kaust.edu.sa

A-stable schemes based on backward difference formulas are very attractive in these situations, especially when the Jacobian of reaction source terms can be suitably and efficiently estimated, e.g. [8–10]. The cost of performing iterations to solve the (local) system of non-linear equations arising from an implicit discretization of the equations of motion is rapidly amortized, as it is specifically offset by the ability to achieve accurate integration using suitably large integration steps.

Unfortunately, the success of a fully implicit treatment of the equations of motion may not be readily generalized to reacting flow models in one or more spatial dimensions. In these settings, diffusion coefficients typically exhibit a non-linear dependence on temperature as well as species concentrations; a fully implicit treatment of reaction and diffusion source terms would thus result in a very large system of non-linear equations, coupling in a non-trivial fashion the state vectors at all grid points. Because the efficient solution of such systems is difficult at best, the development of implicit-explicit (IMEX) approaches [15, 16] was pursued that simultaneously avoid large coupled systems and effectively address the chemical and diffusion stiffness of the governing equations.

In the context of low-Mach-number reacting flow calculations, the deployment of IMEX techniques has in most cases relied on operator-splitting approaches [17–23], specifically based on using fractional stepping to treat chemical source terms separately from diffusion (and advection) terms. These have in particular enabled the implementation of divide-and-conquer strategies, namely by adapting different integration methods to different fractional steps. In operator-split approaches, the treatment of chemical source terms takes the form of spatially-decoupled integrals, which facilitates the implementation of suitable implicit methods. In a high-performance-computing environment, parallel implementation of such implicit techniques is also straightforward. Operator-splitting frameworks have also been exploited to accommodate explicit, extended-stability, predictor-corrector methods [20, 21] to defeat the "diffusion" stiffness of the reacting flow equations. These methods are attractive because their explicit construct naturally avoids the need to solve large systems of coupled equations, and because their extended range of absolute stability along the negative real axis enables the efficient treatment of diffusion terms using large time steps. For instance, for the Runge-Kutta-Chebyshev [24–26] family of integration methods, the size of the absolute stability interval along the real axis grows as the square of the number of stages, S. Thus, for sufficiently large S, treatment of diffusion with an explicit RKC scheme is S times more efficient than using an explicit multistep method. Operator-split approaches combining adaptive stiff solvers for integrating chemical source terms with RKC methods for handling diffusion have proven to be quite effective in direct simulation of reacting flows with detailed chemistry and transport [20, 21].

One of the limitations of operator-split approaches is that the overall order of time integration cannot exceed 2. Another potential symptom of operator splitting in the context of reacting flow calculations is that the predicted states at the end of individual fractional steps can exhibit sizeable oscillations around the true solution. These issues have been examined in detailed by [27] who explored the use of spectrally deferred correction (SDC) approach [28–32] to defeat the stiffness of the equations without relying on operator splitting. In extreme cases involving ignition and extinction phenomena, Strang splitting may fail to predict critical flame limits. This has been widely discussed in Ref. [33, 34], in the context of the determination of the S-curve of a perfectly stirred reactor. A variety of solutions have been consequently developed to avoid such drawbacks, including efficient second-order splitting strategies [35], more sophisticated treatment of the characteristic time scales of the different chemical species involved [36], as well as proper non-split approaches including efficient treatment of Jacobian matrices [37–39].

Inspired by the experiences in [27], the present work tackles the question of whether it is possible to combine, in a non-split fashion, a stiff integrator with an extended stability integrator, and consequently capitalize on the well-established advantages of the former in defeating the stiffness arising from disparate chemical time scales, and of the latter in efficiently treating stiff diffusion terms. Attention is specifically focused on the possibility of developing a hybrid approach for stiff advection-reaction-diffusion equations, combining in a non-split fashion an adaptive stiff solver with the stabilized, second-order RKC scheme [24–26]. In the present implementations, we rely on the adaptive stiff solver from the CVODE package [40], though the methodology can naturally accommodate the use of other stiff integrators. Such hybridization is indeed not straightforward, because the predictor-corrector formulation in RKC involves stage estimates that, in a non-split construct, would be simultaneously affected by all source terms. To overcome this difficulty, we introduce a reformulation of the RKC scheme in terms of stage updates, and consequently enables us to identify the "action" of RKC integrator in a mixed integration framework. In Section 2, we exploit this reformulation to propose a new non-split scheme, and briefly analyze its performance using a stiff, reaction-diffusion model problem for which an analytical solution is available. In Section 3, we outline the implementation of the hybrid scheme to the simulation of the reacting flow equations in the low-Mach-number limit. Applications to a transient ignition and propagation problem are specifically used to contrast predictions obtained using the hybrid scheme with results computed using an operator split approach. Major conclusions are provided in Section 4.

2. Approach

In this section, we outline the construction of a hybrid, non-split, stiff/RKC scheme, namely for the case of a generic reaction-diffusion system:

$$\dot{\mathbf{y}} = D(\mathbf{y}, t) + S(\mathbf{y}, t), \tag{1}$$

where $\mathbf{y}$ is the N-dimensional state vector, $D(\mathbf{y}, t)$ denotes the diffusion term, and $S(\mathbf{y}, t)$ denotes the (stiff) reaction source term. Our goal is to combine an explicit, extended-stability integrator for the diffusion term with (implicit) stiff integration of the reaction source term. For the former, we rely on the stabilitized, second-order, Runge-Kutta-Chebychev (RKC) scheme [20, 21, 25, 26], whereas stiff integration is performed using the CVODE solver, which adaptively applies suitable backward difference formulas (BDFs) [40]. To fix ideas and efficiently describe the construction of the hybrid, non-split scheme, we ignore for the time being the spatial dimension(s), and consequently outline the construction as if the generic problem (1) simply consisted of a system of coupled ODEs.

Note that in its original form [25], the RKC scheme does not readily lend itself to be combined with a stiff integrator. To outline the difficulty, consider the application of the S-stage RKC scheme to advance the solution of the ODE

$$\dot{\mathbf{y}} = f(\mathbf{y}, t), \tag{2}$$

by one time step. Letting $\mathbf{y}^n$ denote the solution at the n-th integration step and Δt

denote the step length, the solution at the individual stages is given by:

$$\begin{aligned}
&\mathbf{Y}^0 = \mathbf{y}^n, \\
&\mathbf{Y}^1 = \mathbf{Y}_0 + \tilde{\mu}_1 \Delta t f_0, \\
&\mathbf{Y}^j = (1-\mu_j-\nu_j)\mathbf{Y}^0 + \mu_j \mathbf{Y}^{j-1} + \nu_j \mathbf{Y}^{j-2} + \tilde{\mu}_j \Delta t f^{j-1} + \tilde{\gamma}_j \Delta t f^0, \quad j = 2, .., S \\
&\mathbf{y}^{n+1} = \mathbf{Y}^S,
\end{aligned} \tag{3}$$

where

$$f^j \equiv f(\mathbf{Y}^j, t_n + c_j \Delta t),$$

whereas $\tilde{\mu}_j$, μ_j, ν_j, $\tilde{\gamma}_j$, and c_j are constants, given analytically in [25], that depend on the number of stages S, and also possibly on the damping parameter ϵ. Typically one sets $\epsilon = 2/13$, as in [25].

In the form given in (3), it is not evident how to incorporate of RKC into a mixed scheme, because one would not be able to readily identify or distinguish the contributions of different sources terms. The difficulty specifically arises because the RKC stages in (3) involve combinations of the state vectors, which in a non-split construction would be affected by all source terms simultaneously.

To overcome this hurdle, a suitable reformulation of RKC integration is first established, namely in terms of solution increments defined according to:

$$\delta \mathbf{Y}^j \equiv \mathbf{Y}^j - \mathbf{Y}^0, \quad j = 0, \ldots, S, \tag{4}$$

where the $\mathbf{Y}^j$ denote the fractional state vectors defined in (3). For the general system in (2), the reformulated S-stage RKC scheme is expressed as:

$$\begin{aligned}
&\delta \mathbf{Y}^0 = 0, \\
&\delta \mathbf{Y}^1 = \tilde{\mu}_1 \Delta t f^0, \\
&\delta \mathbf{Y}^j = \mu_j \delta \mathbf{Y}^{j-1} + \nu_j \delta \mathbf{Y}^{j-2} + \tilde{\mu}_j \Delta t f^{j-1} + \tilde{\gamma}_j \Delta t f^0, \quad j = 2, .., S
\end{aligned} \tag{5}$$

which is indeed quite convenient because the solution *update*, or alternatively the action of the forcing term that is being handled by RKC, can now be explicitly identified.

We exploit the reformulation of the RKC scheme in (5) in developing a hybrid, stiff/extended-stability solver, and outline the construction for the generic reaction diffusion system in (1). The idea is to use (5), with a forcing term, f, corresponding to the diffusion source term, $D(\mathbf{y}, t)$, in order to isolate the action of the RKC on the latter. Thus, the proposed hybrid scheme updates the solution from t_n to $t_{n+1} = t_n + \Delta t$ in S stages, as follows:

(1) Define $\tau_0 \equiv t_n$, $\Delta t_j \equiv c_j \Delta t$, $\tau_j = \tau_0 + \Delta t_j$, $j = 1, \ldots, S$.
(2) Set $\mathbf{Y}^0 = \mathbf{y}^n$, and $\Delta \mathbf{Y}^0 = 0$.
(3) For $j = 1, \ldots, S$, evaluate the diffusion increment according to:

$$\Delta \mathbf{Y}^j = \begin{cases} \tilde{\mu}_1 \Delta t D(\mathbf{Y}^0, \tau_0) & j = 1 \\ \mu_j \Delta \mathbf{Y}^{j-1} + \nu_j \Delta \mathbf{Y}^{j-2} + \tilde{\mu}_j \Delta t D(\mathbf{Y}^{j-1}, \tau_{j-1}) + \tilde{\gamma}_j \Delta t D(\mathbf{Y}^0, \tau_0) & j > 1 \end{cases} \tag{6}$$

and determine the state $\mathbf{Y}^j$ using

$$\mathbf{Y}^j = \mathbf{Y}^0 + \mathcal{S}(\tau_j), \tag{7}$$

where $\mathcal{S}$ denotes the stiff integral

$$\mathcal{S}(\tau_j) \equiv \int_{\tau_0}^{\tau_j} \left[S(\mathbf{y}, t) + \frac{\Delta \mathbf{Y}^j}{\Delta t_j} \right] \mathrm{d}t, \quad j = 1, \ldots, S. \tag{8}$$

(4) Set $\mathbf{y}^{n+1} = \mathbf{Y}^S$.

Remarks

(1) At each stage, an effective diffusion source term is evaluated, using Eq. (6), in such a way that when inserted into the stiff integral associated with the same stage, Eq. (8), the RKC increment is recovered. In the "stage-averaged" approach outline above, the effective diffusion source term is defined as the ratio of the RKC diffusion stage increment divided by the corresponding stage step size.

(2) As briefly outlined in Appendix A, a possible alternative to the stage-averaged representation of the diffusion increment in Eq. (8) may be a linear formulation. The storage requirements are not significantly increased, as well as the numerical cost, with respect to the stage-averaged representation. Numerical tests conducted for model problems [41] revealed that this alternative construction exhibited similar behavior as the one outlined above. For brevity, we omit further discussion of this alternative construction.

(3) In the proposed hybrid scheme, the solution is effectively advanced by making S stiff integrations over increasingly longer sub-intervals, specifically ranging from $c_1 \Delta t \ll \Delta t$ to $c_S \Delta t = \Delta t$.

(4) In each of the integration stages, the stiff integrals involved, Eq. (7), couple the reaction and diffusion terms. In addition, the state vector at the end of the first $(s-1)$ stages is used to compute the corresponding value of the diffusion source term at time τ_j, and to update the diffusion increments. Thus, the hybrid construction does not rely on operator splitting.

(5) At the end of each of the first $(s-1)$ stages, the provisional solution is discarded, and the solution at τ_0 is reloaded, so that the next stiff integral can be evaluated. Because all the stiff integrals have the same starting point, it is advantageous to store the corresponding starting source term and Jacobian at beginning of the first stage, and make these stored values available for the stiff integrals in subsequent stages.

(6) Because the hybrid construction does not rely on operator splitting, the history of the solution from previous integration steps could also be utilized. In other words, the integrals in (7) can take the form of a continuation integration that takes into account the past history of the solution, provided this history is appropriately stored and made available to the solver. Consequently, integration restart could in principle be avoided, and evaluation of new Jacobians would only occur locally as needed.

(7) As outlined above, the hybrid algorithm would at a minimum require the storage of (a) the complete solution state at τ_0; (b) two diffusion source terms, namely $D(\mathbf{Y}^0, \tau_0)$ and $D(\mathbf{Y}^{j-1}, \tau_{j-1})$; and (c) two diffusion increments, $\Delta \mathbf{Y}^{j-1}$ and $\Delta \mathbf{Y}^{j-2}$. Note that we have introduced the notation $\Delta \mathbf{Y}^j$ to refer to the *diffu-*

sion increment defined in Eq. (6), and to distinguish this increment from the stage update given in Eq. (4). Also note that if the original formulation of RKC is used, namely by directly computing solution updates via Eq. (5), it will not be possible to isolate the action of the diffusion term, nor consequently to establish a consistent mixed formulation. To verify this claim, note that the diffusion increments defined in Eq. (6) isolate and store the contribution of the diffusion term *before* the combined stage updates defined in Eqs. (7-8) are evaluated. Consequently, because the stage updates defined in Eqs. (7-8) account simultaneously for both reaction *and* diffusion, the diffusion increment $\Delta\mathbf{Y}^j$ will clearly differ from the combined stage update. It is also clear that $\Delta\mathbf{Y}^j$ may not be recovered from the stage difference $\mathbf{Y}^j - \mathbf{Y}^0$. Thus, the reformulation of RKC and the suitable definition of the diffusion increments in Eq. (6) are in fact key in the construction of a mixed, non-split, stiff/RKC scheme.

(8) In the construction above, the RKC diffusion increment, $\Delta\mathbf{Y}^j$, is spread evenly over the width of the time interval defining the corresponding integration stage, see Eq. (7). Even though it is formally first order, we still expect the numerical scheme to achieve overall second-order accuracy of the RKC integrator. Because the stiff integrator in CVODE uses adaptive time stepping designed to achieve stable integration and to meet user-defined tolerances, we also expect that the overall stability of the mixed scheme to be governed by the critical time step of RKC.

(9) The use of the RKC scheme to handle diffusion is advantageous because the method exhibits an *extended stability* region along the negative real axis, whose size scales with the square of the number of stages (see Eq. (16) below). This enables us to use larger integration steps than in an explicit multistep scheme. When used independently on a pure diffusion problem, the computational gain afforded by RKC scales linearly with the number of stages. In a non-split, stiff/RKC construct however, computational overheads are incurred due to the need to perform a stiff integration for each RKC stage. Despite these additional overheads, the experiences below demonstrate that for fixed level of time integration accuracy, the mixed, non-split stiff/RKC construction remains competitive compared to a Strang-split approach.

(10) In the implementations below, we relied exclusively on the CVODE package to perform the stiff integrals. In doing so, for the case of low-Mach-number combustion application we took advantage of the analytical Jacobian capabilities afforded by TChem [42] to perform the non-linear iterations arising in the application of BDF formulas. As noted in the introduction, however, one can readily use of other time-adaptive stiff integration methods in lieu of CVODE in the framework outlined above.

2.1. A diffusion-reaction model problem

To outline the implementation of the hybrid, non-split approach, we first consider the idealized, transient, one-dimensional, diffusion-reaction system initially proposed in [14]:

$$\frac{\partial u}{\partial t} = \mathcal{D}\frac{\partial^2 u}{\partial x^2} - \mathcal{A}u + v, \tag{9}$$

$$\frac{\partial v}{\partial t} = \mathcal{D}\frac{\partial^2 v}{\partial x^2} - \mathcal{B}v, \tag{10}$$

over the domain $x \in [0, \pi/2]$, with boundary and initial conditions:

$$\left.\frac{\partial u}{\partial x}\right|_{x=0} = \left.\frac{\partial v}{\partial x}\right|_{x=0} = u\left(\frac{\pi}{2}, 0\right) = v\left(\frac{\pi}{2}, 0\right) = 0, \tag{11}$$

$$u(x,0) = 2\cos x, \quad v(x,0) = (A - B)\cos x. \tag{12}$$

The system can be readily recast in the generic form (1), namely by defining the two-dimensional state vector $\mathbf{y}(x,t) \equiv (u(x,t), v(x,t))$, and the diffusion and reaction terms according to

$$D(\mathbf{y},t) = \left(\mathcal{D}\frac{\partial^2 u}{\partial x^2}, \mathcal{D}\frac{\partial^2 v}{\partial x^2}\right), \quad \text{and} \quad S(\mathbf{y},t) = \left(-\mathcal{A}u + v, -\mathcal{B}v\right), \tag{13}$$

respectively.

This is a convenient system because an analytical solution is available,

$$u(x,t) = \left(e^{-(\mathcal{A}+\mathcal{D})t} + e^{-(\mathcal{B}+\mathcal{D})t}\right)\cos x, \tag{14}$$

$$v(x,t) = (\mathcal{A} - \mathcal{B})\, e^{-(\mathcal{B}+\mathcal{D})t}\cos x, \tag{15}$$

and because the diffusion constant, $\mathcal{D}$, and reaction parameters, $\mathcal{A}$ and $\mathcal{B}$, can be tuned to define different behavior regimes. We can readily exploit the form of the analytical solution for this purpose, as the latter immediately indicates the presence of two "modes", with characteristic time scales $(\mathcal{A}+\mathcal{D})^{-1}$ and $(\mathcal{B}+\mathcal{D})^{-1}$.

As we are primarily motivated to investigate stiff combustion problems, we focus on a regime with disparate reaction rates, namely $\mathcal{A} \gg \mathcal{B}$, with diffusion time-scale that is on the same order as the slow reaction, i.e. $\mathcal{D}$ is comparable to $\mathcal{B}$. We thus set $(\mathcal{A}, \mathcal{B}, \mathcal{D}) = (10, 0.1, 0.1)$. One can readily appreciate that the time scales associated with the solution models are indeed disparate, and that accordingly the selected scenario indeed corresponds to a stiff combustion regime.

To simulate the reaction-diffusion system, we first discretize the governing equations using a finite-difference methodology. A uniform grid with $N = 512$ points is used for this purpose. Variables are defined at the node points, and derivatives are approximated using second-order centered differences. The discretized system is integrated using the hybrid scheme, and the integration is carried out from time $t = 0$ to time $t = 1$. The time step is selected to coincide with the critical time step of the RKC scheme, i.e. we set

$$\Delta t = 0.65(S^2 - 1)\frac{\Delta x^2}{4\mathcal{D}} \tag{16}$$

where $\Delta x \equiv \frac{\pi}{2(N-1)}$ is the cell size and S is the number of stages used. The stiff integrator used is the adaptive solver from the DVODE package [43]. The relative error tolerance is fixed at 0, whereas an absolute error tolerance of 10^{-15} is selected.

The accuracy of the numerical solution is measured in terms of the error committed with respect to the analytical solution, whereas temporal order is assessed through a

self-convergence study. Specifically, the error ϵ_u is computed using the l_2 norm,

$$\epsilon_u = \sqrt{\frac{1}{N}\sum_{i=1}^{N}(U_i - u_i)^2}, \tag{17}$$

where N is the number of grid points, U_i and u_i are the numerical and exact solutions of i-th grid point, respectively. The order of self-convergence p_u is computed considering three numerical solutions $\mathbf{U}^{(1)}$, $\mathbf{U}^{(2)}$, and $\mathbf{U}^{(3)}$, computed with time step Δt, $\Delta t/2$, and $\Delta t/4$, respectively. It is obtained from:

$$p_u = \log_2 \sqrt{\frac{\sum_{i=1}^{N}\left(U_i^{(1)} - U_i^{(2)}\right)^2}{\sum_{i=1}^{N}\left(U_i^{(2)} - U_i^{(3)}\right)^2}}. \tag{18}$$

The error ϵ_v and the self-convergence order p_v for $v(x,t)$ are similarly computed.

Figure A1 depicts the analytical solution at the final time, $t = 1$, with the numerical solution obtained using $S = 16$ and $\Delta t = 3.914 \cdot 10^{-4}$. The results indicate an excellent agreement between the computed and analytical solutions. This is further examined in Fig. A2, which illustrates spatial profiles of the absolute difference between the analytical and numerical solution at $t = 1$, for both the u and v components. The errors for both components of the solution never exceed 10^{-6}, and differ by one order of magnitude, consistent with the strengths of the corresponding signals.

Table A summarizes the relative errors e_u and e_v, and the order of self-convergence of the proposed method; provided are results obtained as the number of RKC stages is varied from $S = 2$ to 32. It is seen that for $S \leq 8$, the error is essentially constant. This indicates that in the present setting, when the time step is small, the second-order spatial errors dominate the time integration errors. A similar behavior was observed in [18], in the context of an operator-split treatment of propagating reaction front. As the number of stages is increased to $S = 32$, however, one observes that the impact of time integration on the error at the final is no longer negligible. However, as noted earlier, the solution remains accurate, with small values of absolute and relative errors, as can be appreciated from Figs. A1 and A2. Note that with $S = 32$, the time step $\Delta t = 15.71 \cdot 10^{-3}$, leading to a Fourier number $\mathrm{Fo} \equiv 2\mathcal{D}\Delta t/\Delta x^2 > 332$. Thus, in the present example, the hybrid non-split scheme continues to perform even as the time step exceeds the stability limit of the Euler by two orders of magnitude.

Table A also indicates that at the higher values of S a second-order rate of self-convergence in time is clearly achieved. This is the expected behavior of the hybrid scheme, which incorporates a second-order extended stability method into an "accurate" stiff solver. At low values of S, however, it is seen that the rate of self-convergence in time cannot be observed. The origin of this phenomenon was addressed in [18], and traced back to the nature of the stiff solver which utilizes relative and absolute tolerances to adapt the time step and to set criteria for terminating non-linear iterations. Briefly, as discussed in [18], for very small values of the time step, the error incurred by the extended stability scheme becomes comparable to tolerances used by the stiff solver. Consequently, in this regime the rate of self-convergence in time can no longer be extracted. To verify that this is indeed the case, we repeated the some of the calculations using an absolute tolerance of 10^{-15}. With this refined absolute tolerance value, one

obtains $p_u = 1.97$ and $p_v = 2.03$ with $S = 8$; and $p_u = 2.31$ and $p_v = 2.25$ with $S = 4$.

In summary, based on the results obtained for the simple model problem, we conclude that the hybrid non-split scheme can accurately compute the solution of stiff problems, and that it achieves second-order convergence in time.

3. Hybrid, non-split approach for low-Mach-number combustion

3.1. Governing equations

In the low-Mach-number limit, the equations of motion for a reactive, ideal gas mixture can be expressed as [16–22, 44, 45]:

$$\nabla \cdot \mathbf{v} = -\frac{1}{\rho}\frac{D\rho}{Dt}, \tag{19}$$

$$\frac{\partial \mathbf{v}}{\partial t} = C_u + D_u - \frac{\nabla p}{\rho}, \tag{20}$$

$$\frac{\partial T}{\partial t} = C_T + D_T + S_T, \tag{21}$$

$$\frac{\partial Y_k}{\partial t} = C_k + D_k + S_k, \qquad k = 1, .., N_s, \tag{22}$$

$$p_0 = \rho \bar{R} T, \tag{23}$$

where $\mathbf{v}$ is the fluid velocity, t is time, ρ is the density, T is temperature, Y_k is the mass fraction of species k, N_s is the number of species, p_0 is the thermodynamic pressure, p is the hydrodynamic pressure, $\frac{D}{Dt}$ denotes the material derivative,

$$\bar{R} \equiv \mathcal{R} \sum_{k=1}^{N_s} \frac{Y_k}{W_k} \tag{24}$$

is the specific gas constant, W_k is the molecular weight of species k, whereas $\mathcal{R}$ is the universal gas constant. In the simulations below, we will focus on an open, acoustically-compact domain, and consequently shall treat the thermodynamic pressure, p_0, as constant in time.

The convection, diffusion, and reaction source terms are given by:

$$C_u = -\left(\mathbf{v} \cdot \nabla\right)\mathbf{v}, \qquad D_u = \frac{\nabla \cdot \tau}{\rho}, \tag{25}$$

$$C_T = -\left(\mathbf{v} \cdot \nabla\right)T, \qquad D_T = \frac{\nabla \cdot (\lambda \nabla T)}{\rho c_p} - \frac{1}{c_p}\left(\sum_{k=1}^{N_s} c_{p,k} Y_k \mathbf{V}_k \cdot \nabla\right) T, \tag{26}$$

$$C_k = -\left(\mathbf{v} \cdot \nabla\right)Y_k, \qquad D_k = -\frac{\nabla \cdot (\rho Y_k \mathbf{V}_k)}{\rho}, \tag{27}$$

$$S_T = -\frac{1}{\rho c_p}\sum_{k=1}^{N_s} h_k \dot{\omega}_k, \qquad S_k = \frac{\dot{\omega}_k}{\rho}. \tag{28}$$

where τ is the Newtonian stress tensor [21], λ is the mixture thermal conductivity, c_p is the mixture specific heat at constant pressure, $c_{p,k}$ specific heat at constant pressure of species k, whereas $\mathbf{V}_k$, h_k, and $\dot{\omega}_k$ respectively denote the diffusion velocity, the specific

enthalpy and mass production rate of the k-th species. Soret and Dufour effects are ignored. We will rely on a mixture-averaged formulation for species diffusion, in which the diffusion velocity, $\mathbf{V}_k$, is expressed as:

$$\mathbf{V}_k = -\frac{D_{m,k}}{Y_k}\left(\nabla Y_k + \frac{Y_k}{W}\nabla W\right), \tag{29}$$

where $D_{m,k}$ is the mass diffusivity of the k-th species, and W is the molecular weight of the mixture. The diffusion coefficients involved are computed using the dipole-reduced formalism implemented from [46]. The TChem library [42] is used to compute the chemical source terms, and the Jacobian involved in the stiff integration of the reaction terms; it is also used to compute the thermodynamic properties, as expressed using NASA polynomials [47].

3.2. Operator-split and hybrid non-split formulations

The present hybrid non-split, low-Mach solver is constructed by modifying the operator-split scheme from [21]. The modification specifically targets the integration of the evolution equations of temperature and species mass fractions. For this reason, the scheme is referred as non-split, even though the pressure projection algorithm is retained. To clearly present the modifications, we first provide a brief oultine of the methodology developed in [21], and then discuss in more detail the symmetrically-split treatment of the temperature and species evolution equations from [21], and the presently-developed hybrid non-split treatment of the corresponding system.

The numerical scheme from [21] is based on a finite-difference methodology. Field variables are discretized using a staggered grid, with scalars (p, ρ, T, Y_k) represented at cell centers whereas the velocity components are defined at the cell faces. The equations are approximated using fourth-order differences, and the discretized equations are advanced in time using a predictor-corrector methodology that can be briefly summarized as follows:

S1. A provisional value of the density at the new time level is obtained by explicit extrapolation, and a provisional value of the velocity field is determined by: (a) explicitly integrating the pressure-split momentum equations, (b) determining a discrete pressure distribution by solving a pressure Poisson equation (PPE), and (a) based on this pressure distribution, applying a pressure correction to the velocity field from step (a).

S2. Species mass fractions and temperature are advanced to the next time level using a symmetrically-split methodology, and the density at the new time level is obtained from the equation of state. The splitting can be realized in two versions. In the first one, the diffusion term is integrated over one half of the integration step, followed by a full step integration of the reaction term, and finally integration of the diffusion term over one half step. This is referred to as diffusion-reaction-diffusion (DRD) splitting. Alternatively, integration of the reaction source is performed over two half steps, conducted before and after full-step integration of the diffusion source term. This is referred to as reaction-diffusion-reaction (RDR) splitting.

S3. Velocity field at the new time level is obtained by: (i) a quasi-Crank-Nicolson integration of the pressure-split momentum equations, specifically involving the provisional velocity values from step S1(a) and the updated scalar values from S2;

(ii) solving a PPE, involving the updated scalar distribution from S2; and (iii) based on the resulting pressure distribution, applying a pressure correction to the velocity field from step (i).

This methodology was implemented in an in-house code [21], which served as a starting point for the present development. Note that the solver also incorporates an adaptive mesh refinement machinery [21], but the latter is not utilized in the present demonstrations.

3.2.1. Hybrid non-split approach

The hybrid approach from Section 2 can be adapted to low-Mach reactive flows simulations, and used in place of the Strang-splitting approach to perform stage 2 of the method in Section 3.2. Again, the update of the solution from the n-th to the $n+1$-th time step consists in S sequential stages:

$$\begin{aligned} T^j &= T^0 + \int_{\tau_0}^{\tau_j} \left[S_T + \frac{\Delta T^j}{\Delta t_j} \right] \mathrm{d}t, \\ Y_k^j &= Y_k^0 + \int_{\tau_0}^{\tau_j} \left[S_k + \frac{\Delta Y_k^j}{\Delta t_j} \right] \mathrm{d}t, \quad k = 1, \ldots, N_s \end{aligned} \tag{30}$$

where $\tau_0 = t_n$, $\tau_j = \tau_0 + c_j \Delta t$, $\Delta t_j = c_j \Delta t$. As in the split scheme, the stiff integrals appearing in the stage updates above are performed using the CVODE solver [40]. Following the notations introduced in Section 2 and 3.1, the RKC individual stage updates featuring in the stiff integrals can be expressed as:

$$\begin{aligned} &\Delta T^0 = 0, && \Delta Y_k^0 = 0, \\ &\Delta T^1 = \tilde{\mu}_1 \Delta t f_T^0, && \Delta Y_k^1 = \tilde{\mu}_1 \Delta t f_k^0, \\ &\Delta T^j = \mu_j \Delta T^{j-1} + \nu_j \Delta T^{j-2} + \tilde{\mu}_j \Delta t f_T^{j-1} + \tilde{\gamma}_j \Delta t f_T^0, \quad j = 2, .., S \\ &\Delta Y_k^j = \mu_j \Delta Y_k^{j-1} + \nu_j \Delta Y_k^{j-2} + \tilde{\mu}_j \Delta t f_k^{j-1} + \tilde{\gamma}_j \Delta t f_k^0, \quad j = 2, .., S \end{aligned} \tag{31}$$

where

$$\begin{aligned} f_T^0 &= C_T(T^0, Y_1^0, .., Y_{N_s}^0) + D_T(T^0, Y_1^0, .., Y_{N_s}^0), \\ f_k^0 &= C_k(T^0, Y_1^0, .., Y_{N_s}^0) + D_k(T^0, Y_1^0, .., Y_{N_s}^0), \\ f_T^{j-1} &= C_T(T^{j-1}, Y_1^{j-1}, .., Y_{N_s}^{j-1}) + D_T(T^{j-1}, Y_1^{j-1}, .., Y_{N_s}^{j-1}), \\ f_k^{j-1} &= C_k(T^{j-1}, Y_1^{j-1}, .., Y_{N_s}^{j-1}) + D_k(T^{j-1}, Y_1^{j-1}, .., Y_{N_s}^{j-1}). \end{aligned} \tag{32}$$

Finally note that (i) the last (S) stage integration yields the solution at the next level, i.e. $T^{n+1} = T^S$, and $Y_k^{n+1} = Y_k^S$, $k = 1, \ldots, N_s$; (ii) the RKC increments in Eq. (31–32) now account for the combined effects of convection and diffusion.

Note that it is straightforward to directly contrast the behavior of the RDR-split and hybrid non-split schemes, because in both formulations the RKC treatment of diffusion and convection uses the same (global) time step. In particular, the time step restrictions associated with the explicit, extended-stability integration are also the same. This would evidently not be the case had we selected a DRD splitting, which would have introduced an additional layer of complexity in the analysis.

3.3. Application of the hybrid approach

The hybrid method is applied to simulate the low-Mach number reacting flow equations, namely for the case of a freely propagating one-dimensional premixed methane-air flame. The chemical model is described by GRI-Mech 1.2 mechanism [48], which involves 32 species and 177 elementary reactions. The integration time of the simulation is 20 ms. The computational domain is $L_x = 0.015$ m long, and is discretized using a uniform grid having 768 cells; accordingly, the spatial cell size is $\Delta x = 1.953 \cdot 10^{-5}$ m. The starting condition consists in a quiescent stoichiometric mixture of methane-air gas at $T = 300$ K and ambient pressure. At $x = 0$, a vanishing velocity boundary condition is used, whereas outflow boundary conditions are imposed at $x = 0.015$ m.

An idealized spark is used to ignite the mixture, modeled in terms of a transient source term, H_T, added to the RHS of Eq. (21). The ignition source is active from $t = 0$ ms to $t = 0.4$ ms:

$$H_T = \frac{\dot{h}}{\rho c_p}, \tag{33}$$

where

$$\dot{h} \equiv \begin{cases} 9.1 \cdot 10^9\,\mathrm{W/m^3} & x_H - \delta_H \le x \le x_H + \delta_H,\ T(x_H) \le 2500\,\mathrm{K} \\ 2.7 \cdot 10^9\,\mathrm{W/m^3} & x_H - \delta_H \le x \le x_H + \delta_H,\ T(x_H) > 2500\,\mathrm{K} \\ 0 & \text{otherwise} \end{cases}. \tag{34}$$

The spark is centered at $x_H = 0.012$ m, and the spark half-width $\delta_H = 9.77 \cdot 10^{-5}$ m. The heat source is designed to prevent excessively high temperature values, which would lead to substantial restriction of the integration time step during the ignition transient. This is the case because sharp fronts develop during the ignition phase, and because transport coefficients increase rapidly with temperature. The design of the source properties was motivated by our desire to conduct a systematic assessment of the performance of the hybrid scheme, using a fixed time step that is valid for the entire simulation interval, and that is not overly restricted by stability conditions associated with explicit treatment of the transport terms.

Figure A3 shows instantaneous profiles of the temperature and OH mass fraction, both during the ignition transient and subsequent flame propagation regime. Also plotted for comparison are results obtained using a Strang-split, RDR scheme. In both cases, the global integration time step is $\Delta t = 400$ ns, RKC integration uses $S = 8$ stages, and the relative and absolute tolerances of the stiff integrator are fixed to 10^{-8} and 10^{-14}, respectively. Comparing the results obtained with the hybrid and Strang-split schemes shows that both approach yield similar predictions. In particular, there does not appear to be significant differences in the details of the concentration profiles, including peak and front locations as well as peak concentration amplitudes. Very small differences can however be discerned near the right boundary of the domain, suggesting that near outflow boundaries the solution may be affected by the properties of the time integration scheme. These differences are more visible in the OH profiles, originate during the ignition transient ($t \le 4$ ms) but persist at later times even as an essentially steady propagating front is established. Overall, however, these differences are insignificant, and the reaction zone structures illustrated in Fig. A3 are in excellent agreement.

As suggested by [27], the effect of operator splitting can be appreciated by visualizing the evolution of the solution during the intermediate stages of a single time step. We

repeated the same analysis for the solutions shown in Fig. A3, namely for the Strang-split RDR scheme and the hybrid method. The results are plotted in Fig. A4. The graphs represent the mass fractions of OH and C_2H_5 at fixed spatial locations, selected to be the peak locations of these concentration profiles at $t = 20$ ms. Results obtained using the hybrid approach as represented using solid lines, whereas the open squares and diamonds depict the solution computed at the end of of the first and second stiff reaction half-steps of the Strang-split scheme. The solid squares reflect the intermediate values of the solution at the end of the individual stages of the RKC treatment of the diffusion and advection terms. It is clear that the non-split solution exhibits smooth behavior, which reflects steadily evolving balance between reaction, diffusion and advection terms. In contrast the Strang-split solution exhibits appreciable oscillations around the smooth evolution predicted by the non-split scheme. One observes that in the split scheme a rapid jump occurs during the first reaction half-step. This jump is more pronounced in the case of OH, causing the split solution to cross-over the smooth curve predicted by the non-split scheme. In the case of C_2H_5, the first reaction half-step is seen to cause a small change, causing the split scheme partial update to move away from the non-split prediction. For both OH and C_2H_5, this is followed by a gradual readjustment as diffusion and advection source terms are accounted for using RKC integration, and during this readjustment the split solution crosses over that non-split prediction. In the second stiff reaction half-step, a jump also occurs; for OH, the second reaction half-step leads to a moderate change in the OH concentration, but the change is significantly more pronounced in the case of C_2H_5. In both cases, however, at the end of the full integration step the solution is brought closer to the non-split update. Though the split and non-split solutions at the end of the integration steps are close to each other, splitting errors stiff manifest themselves as a small systematic shift between the curves. Another manifestation of splitting errors is that changes occurring during fractional step updates have amplitudes that can substantially exceed the corresponding full step update.

A simplified analysis was conducted in order to provide a quantitative description of the effect of operator splitting. To this end, a reference solution was first computed, namely using the non-split scheme, with $S = 2$ stages, and a very fine time step $\Delta t =$ 1 ns. To limit their potential impact on the analysis, the relative tolerance and absolute tolerance used by the stiff integrator were reduced to 10^{-10} and 10^{-16}, respectively. The initial condition used in the simplified analysis was adapted from a non-split solution at $t = 20$ ms, i.e. at time when the ignition transient has decayed and a self-propagating front has been established. Starting from this initial condition, several computations were performed using the split and non-split schemes, varying the number of stages and the time step, yet keeping the latter much larger than the time step used by the reference solution.

Of course, selection of the global time step in both the hybrid scheme and split-scheme computations must adhere to stability restrictions. Because the stiff integrator uses an adaptive stepping strategy, in the present setup the prevailing restrictions arise due to the explicit treatment of diffusion and convection terms. So long as advection velocities are small, the global time step is restricted by the stability limit of the RKC treatment of diffusion. As noted earlier, the latter increases essentially quadratically with the number of stages, S. In the present step, one observes large changes in the peak flow velocities as the simulation progresses. Specifically, in the early stages of the computations, large flow velocities develop when the ignition source is active. In these early stages, the global time step can be selected to coincide with the critical time step associated with the RKC treatment of diffusion so long as the number of stages $S \leq 8$.

For higher values of S, the stable treatment of convection becomes the limiting factor, which restricts the global time step to $\Delta t = 2.4\,\mu$s and $\Delta t = 1.6\,\mu$s for the hybrid scheme and split RDR schemes respectively. At later stages of the simulation, after the ignition source has been turned off and a self-propagating front is established, the peak flow velocities drop sufficiently to enable us to pick the global time step close to the RKC stability limit for $2 \leq S \leq 32$. In this regime, stable calculations (not shown) were in fact performed using the hybrid scheme with a global time of 800 ns with $S = 8$; $3.2\,\mu$s with $S = 16$; and $10\,\mu$s with 32. Similarly, stable split-scheme computations were performed with a global time step of 700 ns with $S = 8$; $1.8\,\mu$s with $S = 16$ and $9\,\mu$s with $S = 32$. As expected, the observed stability limits are similar for the two methods, though evidently the hybrid scheme can tolerate slightly larger global time steps. This is due to the stable treatment of reaction and diffusion in the hyrbid scheme, whereas the Strang-split scheme may benefit only from the stable treatment of diffusion in the fractional step updates.

In the analysis below, we have opted to follow a simplified approach to select the global time step. Specifically, global time step values are selected that enable stable computations over the entire simulation interval, namely starting from a cold mixture. We thus report results of computations performed using the hybrid non-split and the RDR split schemes $S = 2$ with $\Delta t = 20$ ns; $S = 4$ with $\Delta t = 100$ ns; $S = 8$ with $\Delta t = 400$ ns; $S = 16$ with $\Delta t = 1$ μs. Note that this allows us to simplify the analysis, namely by avoiding the use of elaborate adaptive time stepping strategies, and also to conduct a conservative assessment of the performance of the proposed non-split integration method. Note that with the simplified approach adopted, in the range $S > 16$ the time step could not be increased by increasing the number of stages, namely due to constraints associated with stable treatment of advection. With the time step fixed at $\Delta t = 1$ μs, we performed computations with $S = 32$ (not shown), and observed that the relative error, estimated with respect to the reference solution, did not appreciably change by increasing S.

Figure A5 shows the relative difference in the peak values of OH and C_2H_5 mass fractions at the end of the simulation interval. Shown are results obtained using the hybrid non-split and the split RDR scheme at all $(S, \Delta t)$ pairs considered. The relative difference is very small at small of values of the time step, and increases monotonically as Δt and S are increased. In particular, the expected second-order behavior is observed for the larger values of Δt. Consistent with our observations in the previous section, the estimated relative errors for the hybrid scheme are nearly one order of magnitude smaller than the corresponding estimates obtained using the split solution using the same values of S and Δt. These observations are in agreement with analogous findings in [20] and [27].

By construction, the solution update in the hybrid scheme takes the form of repeated evaluation of stiff integrals over time sub-intervals of increasing length, corresponding to the stages of the RKC integrator. This may inherently involve significant overheads, because the adaptive BDF approach involved in the stiff integration requires Jacobian evaluations as needed in the associated Newton iterations. In the present implementation, we have restricted our effort in minimizing the overheads of the repeated stiff integrals by storing and re-using the starting values of the source terms and the Jacobian of the reaction source term. Despite the focused nature of our optimization effort, we briefly examine the impact of the computational efficiency of the hybrid scheme, namely by examining the computational cost of the non-split scheme simulations in light of the surrogate error results presented in Fig. A5. To this end, we recorded the CPU time required by the hybrid and split RDR scheme, running all the simulations

as purely serial. The results indicated that for the same number of stages, S, the hybrid scheme as implemented requires appreciably more CPU time than the split RDR scheme. Specifically, for $S = 8$, the CPU time of the hybrid scheme is 1.4 times larger than that of the split scheme, whereas for $S = 16$ the hybrid scheme requires a CPU time that is 4.5 larger than that of the split scheme. Thus, the overheads associated with the hybrid formulation can be substantial. On the other hand, from the perspective of achieving a target relative error (as defined earlier), the hybrid scheme is notably better performing. For instance, to achieve a relative error of 10^{-5} for the mass fraction of C_2H_5, the split RDR scheme will require computations at small time step and number of stages, specifically $\Delta t = 20$ ns with $S = 2$. To achieve the same target, on the other hand, the hybrid scheme can afford the use of larger time step and RKC stages, specifically $\Delta t = 400$ ns with $S = 8$. Comparing these calculations, we find that the hybrid scheme computations are 6 times faster than the corresponding split scheme computations. We thus conclude that the hybrid approach can offer performance gains over the operator-split formulation in order to achieve similar error levels. Of course, additional performance improvements in the hybrid approach could be sought using more elaborate treatments, for instance as in deferred correction approach [27]. Such improvements will be pursued in future work, and reported elsewhere.

4. Conclusions

A new strategy was developed for coupling, in a non-split fashion, stiff integration methods with explicit, extended-stability, predictor-corrector methods. Attention was specifically focused on coupling the stiff solver from the CVODE package with the stabilized Runge-Kutta-Chebyshev scheme. To enable a mixed non-split construction, a reformulation of the RKC scheme was performed, expressing the individual stages as solution updates that enable us to isolate the impact of the forcing term that is being handled by the predictor-corrector scheme. This reformulation was consequently exploited to design a hybrid non-split approach, consisting in sequential stiff integrations over increasingly large sub-intervals, in which the reaction source term is handled directly by the stiff solver whereas the RKC treatment of the diffusion term is accounted for in terms a stage-averaged source term representation.

The hybrid solver was initially tested for an idealized, stiff reaction-diffusion model problem, discretized in space using second-order centered differences. The numerical solution was tested against the analytical solution, and the behavior of prediction errors was assessed as the number of RKC stages is systematically increased while maintaining the time at the critical diffusion stability limit. Specifically, the number of RKC stages was varied from 2 to 32, enabling us to consider a wide range of Fourier numbers, ranging from near unity to over 332. Analysis of computed results indicated that the solution errors were very small in the entire range of time steps considered, and that spatial errors were dominant except when the number of RKC stages becomes very large. A self-convergence study was also performed in order to assess the behavior time integration errors. As anticipated, second-order convergence was observed at the larger time step values considered. However, for very small Δt, the order of self convergence could not be observed due tolerances used by the stiff solver.

To assess the impact of splitting errors in a relevant setting, the hybrid scheme was applied to simulate a one-dimensional, freely propagating methane-air flame, and the results were compared to predictions obtained using a Strang-split approach. Both the hybrid and split schemes rely on the same low-Mach-number reacting formulation

accounting for detailed kinetics and transport, utilize the same computational grids, and the same fourth-order discretization of the governing equations. Computed results indicated that the solutions obtained using non-split and Strang-split schemes are close to each other, both during ignition transients as well as steady propagation, in the wide range of the number of RKC stages considered. Whereas both approaches exhibited second-order time convergence, the analysis showed that the solutions obtained using the String-split approach was characterized by sizable oscillations and relaxations during sub-steps, unlike the solutions obtained using the hybrid non-split approach which reveal smooth behavior across internal stages and global time steps. Consistent with these observations, the analysis also revealed that, for the same global time step, the estimated time integration errors in the non-split approach are significantly smaller than in the Strang-split scheme. The reduction in time integration error achieved by the non-split scheme over the Strang-split construction becomes more appreciable at larger time steps, which mitigates the larger computational overhead associated with stiff integration over individual stages.

The present work has focused on developing the machinery for constructing hybrid integrator combining in a non-split fashion a stiff solver with an extended-stability predictor corrector method. Attention was specifically restricted to the second-order RKC scheme. Success in avoiding splitting errors naturally raises the question whether such hybridization is possible using a higher-order extended-stability scheme (e.g. [49, 50]). This would likely warrant a deeper investigation of how the extended-stability stage updates are represented in the sequential stiff integrations, specifically to maintain a higher order in time behavior. Different avenues could be possible, including interpolation-based approaches [25] and higher-order representations such as those outlined in the Appendix. It would also be worthwhile to explore further enhancement of computational efficiency, for instance through suitable storage of Jacobian and source terms, as well as developing means of exploiting available stage updates to defeat the stiffness of subsequent stages. These issues will be the focus of future work.

Acknowledgements

Research reported in this publication was supported by research funding from King Abdullah University of Science and Technology (KAUST). Sandia National Laboratories is a multimission laboratory managed and operated by National Technology and Engineering Solutions of Sandia, LLC., a wholly owned subsidiary of Honeywell International, Inc., for the U.S. Department of Energy's National Nuclear Security Administration under contract DE-NA-0003525. The views expressed in this paper do not necessarily represent the views of the U.S. Department of Energy or the United States Government.

References

[1] W. Hung, C. Chen, and J. Haviland, *Numerical solutions of reactive fluid flows during postignition transients in hybrid rocket systems*, Journal of Computational Physics 9 (1972), pp. 167–193.

[2] R. Alexander, *Diagonally implicit Runge–Kutta methods for stiff ODE's*, SIAM Journal on Numerical Analysis 14 (1977), pp. 1006–1021.

[3] G. Otey and H. Dwyer, *Numerical study of the interaction of fast chemistry and diffusion*, AIAA Journal 17 (1979), pp. 606–613.

[4] E. Kansa, *An algorithm for multidimensional combusting flow problems*, Journal of Computational Physics 42 (1981), pp. 152–194.
[5] K. Radhakrishnan, *Comparison of numerical techniques for integration of stiff ordinary differential equations arising in combustion chemistry* (1984). NASA-TP-2372.
[6] F. Benkhaldoun and B. Larrouturou, *A finite element adaptive investigation of curved stable and unstable flame front*, Computer Methods in Applied Mechanics and Engineering 76 (1989), pp. 119–134.
[7] R.J. LeVeque and H.C. Yee, *A study of numerical methods for hyperbolic conservation laws with stiff source terms*, Journal of Computational Physics 86 (1990), pp. 187–210.
[8] R.J. Kee, L.R. Petzold, M.D. Smooke, and J.F. Grcar, *Implicit methods in combustion and chemical kinetics modeling*, in *Multiple Time Scales*, Elsevier, 1985, pp. 113–144.
[9] A. Ostermann, P. Kaps, and T. Bui, *The solution of a combustion problem with Rosenbrock methods*, ACM Transactions on Mathematical Software (TOMS) 12 (1986), pp. 354–361.
[10] S. Cho, R. Yetter, and F. Dryer, *A computer model for one-dimensional mass and energy transport in and around chemically reacting particles, including complex gas-phase chemistry, multicomponent molecular diffusion, surface evaporation, and heterogeneous reaction*, Journal of Computational Physics 102 (1992), pp. 160–179.
[11] G.J. Wilson and R.W. MacCormack, *Modeling supersonic combustion using a fully implicit numerical method*, AIAA journal 30 (1992), pp. 1008–1015.
[12] A. Berkenbosch, E. Kaasschieter, R. Klein, *et al.*, *Detonation capturing for stiff combustion chemistry*, Combustion Theory and Modelling 2 (1998), pp. 313–348.
[13] M. Valorani and D.A. Goussis, *Explicit time-scale splitting algorithm for stiff problems: auto-ignition of gaseous mixtures behind a steady shock*, Journal of Computational Physics 169 (2001), pp. 44–79.
[14] C. Chou, Y. Zhang, R. Zhao, and Q. Nie, *Numerical methods for stiff reaction-diffusion systems*, Discrete and Continuous Dynamical Systems 7 (2007), p. 515.
[15] U.M. Ascher, S.J. Ruuth, and B.T. Wetton, *Implicit-explicit methods for time-dependent partial differential equations*, SIAM Journal on Numerical Analysis 32 (1995), pp. 797–823.
[16] H.N. Najm, P.S. Wyckoff, and O.M. Knio, *A semi-implicit numerical scheme for reacting flow: I. stiff chemistry*, Journal of Computational Physics 143 (1998), pp. 381–402.
[17] A.G. Tomboulides, J.C.Y. Lee, and S.A. Orszag, *Numerical Simulation of Low Mach Number Reactive Flows*, Journal of Scientific Computing 12 (1997), pp. 139–167.
[18] O.M. Knio, H.N. Najm, and P.S. Wyckoff, *A semi-implicit numerical scheme for reacting flow: II. Stiff, operator-split formulation*, Journal of Computational Physics 154 (1999), pp. 428–467.
[19] M.S. Day and J.B. Bell, *Numerical simulation of laminar reacting flows with complex chemistry*, Combustion Theory and Modelling 4 (2000), pp. 535–556.
[20] H.N. Najm and O.M. Knio, *Modeling low Mach number reacting flow with detailed chemistry and transport*, Journal of Scientific Computing 25 (2005), p. 263.
[21] C. Safta, J. Ray, and H. Najm, *A high-order low-Mach number AMR construction for chemically reacting flows*, Journal of Computational Physics 229 (2010), pp. 9299–9322.
[22] O. Desjardins, G. Blanquart, G. Balarac, and H. Pitsch, *High order conservative finite difference scheme for variable density low Mach number turbulent flows*, Journal of Computational Physics 227 (2008), pp. 7125–7159.
[23] A. Cuoci, A. Frassoldati, T. Faravelli, and E. Ranzi, *Numerical modeling of laminar flames with detailed kinetics based on the operator-splitting method*, Energy & Fuels 27 (2013), pp. 7730–7753.
[24] P.J. van Der Houwen and B.P. Sommeijer, *On the Internal Stability of Explicit, m-Stage Runge-Kutta Methods for Large m-Values*, ZAMM - Zeitschrift für Angewandte Mathematik und Mechanik 60 (1980), pp. 479–485.
[25] B. Sommeijer, L. Shampine, and J. Verwer, *RKC: An explicit solver for parabolic PDEs*, Journal of Computational and Applied Mathematics 88 (1998), pp. 315–326.
[26] J.G. Verwer, B.P. Sommeijer, and W. Hundsdorfer, *RKC time-stepping for advection–*

diffusion–reaction problems, Journal of Computational Physics 201 (2004), pp. 61–79.
[27] A. Nonaka, J. Bell, M. Day, C. Gilet, A. Almgren, and M. Minion, *A deferred correction coupling strategy for low Mach number flow with complex chemistry*, Combustion Theory and Modelling 16 (2012), pp. 1053–1088.
[28] A. Dutt, L. Greengard, and V. Rokhlin, *Spectral deferred correction methods for ordinary differential equations*, BIT Numerical Mathematics 40 (2000), pp. 241–266.
[29] A. Bourlioux, A.T. Layton, and M.L. Minion, *High-order multi-implicit spectral deferred correction methods for problems of reactive flow*, Journal of Computational Physics 189 (2003), pp. 651–675.
[30] A.T. Layton and M.L. Minion, *Conservative multi-implicit spectral deferred correction methods for reacting gas dynamics*, Journal of Computational Physics 194 (2004), pp. 697–715.
[31] M. Emmett, W. Zhang, and J.B. Bell, *High-order algorithms for compressible reacting flow with complex chemistry*, Combustion Theory and Modelling 18 (2014), pp. 361–387.
[32] W.E. Pazner, A. Nonaka, J.B. Bell, M.S. Day, and M.L. Minion, *A high-order spectral deferred correction strategy for low Mach number flow with complex chemistry*, Combustion Theory and Modelling 20 (2016), pp. 521–547.
[33] Z. Lu, H. Zhou, S. Li, Z. Ren, T. Lu, and C.K. Law, *Analysis of operator splitting errors for near-limit flame simulations*, Journal of Computational Physics 335 (2017), pp. 578–591.
[34] H. Wu, P.C. Ma, and M. Ihme, *Efficient time stepping for reactive turbulent simulations with stiff chemistry*, in *2018 AIAA Aerospace Sciences Meeting*. 2018, p. 1672.
[35] Z. Ren and S.B. Pope, *Second-order splitting schemes for a class of reactive systems*, Journal of Computational Physics 227 (2008), pp. 8165–8176.
[36] Y. Gao, Y. Liu, Z. Ren, and T. Lu, *A dynamic adaptive method for hybrid integration of stiff chemistry*, Combustion and Flame 162 (2015), pp. 287–295.
[37] Q. Xie, Z. Xiao, and Z. Ren, *A spectral radius scaling semi-implicit iterative time stepping method for reactive flow simulations with detailed chemistry*, Journal of Computational Physics 368 (2018), pp. 47–68.
[38] J.F. MacArt and M.E. Mueller, *Semi-implicit iterative methods for low mach number turbulent reacting flows: Operator splitting versus approximate factorization*, Journal of Computational Physics 326 (2016), pp. 569–595.
[39] B. Savard, Y. Xuan, B. Bobbitt, and G. Blanquart, *A computationally-efficient, semi-implicit, iterative method for the time-integration of reacting flows with stiff chemistry*, Journal of Computational Physics 295 (2015), pp. 740–769.
[40] S.D. Cohen, A.C. Hindmarsh, P.F. Dubois, *et al.*, *CVODE, a stiff/nonstiff ODE solver in C*, Computers in Physics 10 (1996), pp. 138–143.
[41] Alzahrani, Hasnaa H, *Mixed, Nonsplit, Extended Stability, Stiff Integration of Reaction Diffusion Equations*, Master's thesis, King Abdullah University of Science and Technology, 2016.
[42] C. Safta, H.N. Najm, and O. Knio, *TChem – A Software Toolkit for the Analysis of Complex Kinetic Models*, Sandia Report, SAND2011-3282 (2011).
[43] P.N. Brown, G.D. Byrne, and A.C. Hindmarsh, *Vode: A variable-coefficient ode solver*, SIAM journal on scientific and statistical computing 10 (1989), pp. 1038–1051.
[44] R.G. Rehm and H.R. Baum, *The equations of motion for thermally driven, buoyant flows*, Journal of Research of the NBS 83 (1978), p. 2.
[45] Majda, Andrew and Sethian, James, *The derivation and numerical solution of the equations for zero Mach number combustion*, Combustion Science and Technology 42 (1985), pp. 185–205.
[46] P.H. Paul, *DRFM: A new package for the evaluation of Gas-phase transport properties*, Tech. Rep., Sandia Labs., Livermore, CA (United States), 1997.
[47] B.J. McBride, S. Gordon, and M.A. Reno, *Coefficients for calculating thermodynamic and transport properties of individual species* (1993). NASA Technical Memorandum 4513.
[48] M. Frenklach, H. Wang, C. Yu, M. Goldenberg, C. Bowman, R. Hanson, D. Davidson, E. Chang, G. Smith, D. Golden, *et al.*, *GRI-Mech 1.2, An Optimized Detailed Chemical*

Reaction Mechanism for Methane Combustion, Tech. Rep., Gas Research Institute, 1995.
[49] S. O'Sullivan, *A class of high-order Runge–Kutta–Chebyshev stability polynomials*, Journal of Computational Physics 300 (2015), pp. 665–678.
[50] A. Abdulle, *Fourth order Chebyshev methods with recurrence relation*, SIAM J. Sci. Comput. 23 (2002), pp. 2041–2054.

Appendix A. Alternative formulation of the hybrid scheme

In the hybrid formulation sketched in Section 2, the effect of the RKC stage update is accounted for using a constant (stage-averaged) source term. The amplitude of this average source term is determined so that the stiff integration yields the desired RKC stage update at the end of the corresponding stiff integration period. In this Appendix, we outline an alternative representation, which specifically uses a linear representation of the RKC update in the stiff integral.

To outline this construction, let us for the time being ignore the reaction source term, and consider fitting the evolution of the j-th stage solution via a parabola between τ_0 and τ_j. Following the notation in Section 2, we seek a representation of the form

$$\mathbf{Y}^j(t) = \mathbf{Y}^0 + A^j t + B^j t^2. \tag{A1}$$

The (vector) quantities A^j and B^j are constrained to satisfy the following relations:

$$\begin{aligned} \mathbf{Y}^j(\tau_j) &= \mathbf{Y}^0 + \Delta\mathbf{Y}^j = \mathbf{Y}^0 + A^j\tau_j + B^j\tau_j^2, \\ \frac{\mathrm{d}\mathbf{Y}^j}{\mathrm{d}t}(\tau_0) &= A^j + 2B^j\tau_0 = D(\mathbf{Y}^0, t_n). \end{aligned} \tag{A2}$$

Solving for A^j and B^j one obtains:

$$A^j = \frac{D(\mathbf{Y}^0, t_n)\tau_j^2 - 2\tau_0\Delta\mathbf{Y}^j}{\tau_j^2 - 2\tau_0\tau_j}, \qquad B^j = \frac{\Delta\mathbf{Y}^j - A^j\tau_j}{\tau_j^2}. \tag{A3}$$

This suggests replacing the averaged diffusion representation in Eq. (8) with an alternative linear term, namely according to:

$$\mathcal{S}(\tau_j) = \int_{\tau_0}^{\tau_j} \left[S(y,t) + A^j + 2B^j t\right] \mathrm{d}t. \tag{A4}$$

With other elements of the algorithm given in Section 2 remaining the same, this yields an alternative formulation of the hybrid scheme.

Table A1. Fourier symbol Fo, RMS error (Eq. (17)), and order of self-convergence (Eq. (18)) for different values of the number of RKC stages, S. The errors are computed for the solution the diffusion-reaction model problem at the final time, $t = 1$. The relative and absolute tolerances for the stiff solver are zero and 10^{-15} respectively.

S	$\Delta t \cdot 10^3$	Fo	$\epsilon_u \cdot 10^9$	$\epsilon_v \cdot 10^9$	p_u	p_v
2	0.046	0.974	45.07	446.19	-0.91	-0.94
4	0.23	4.868	45.05	446.60	-1.79	-2.49
8	0.96	20.32	45.11	446.66	2.49	2.23
16	3.91	82.75	45.86	454.74	1.99	2.01
32	15.71	332.5	57.23	577.11	2.01	2.00

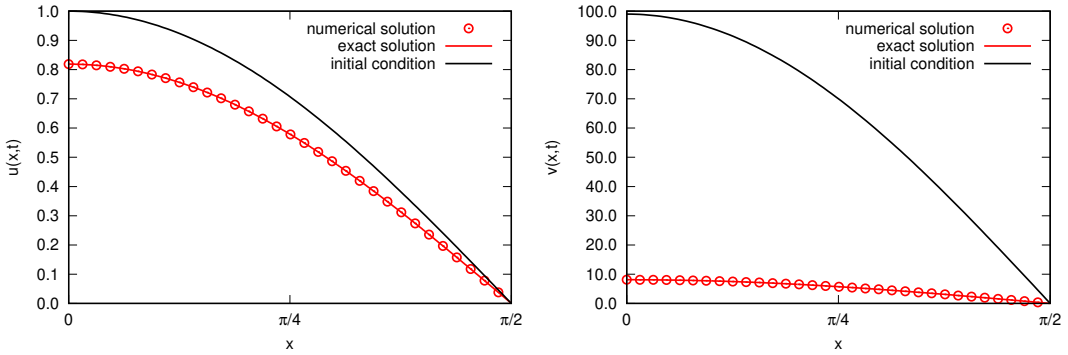

(a) $u(x,t)$ (b) $v(x,t)$

Figure A1. Spatial profiles of the analytical (red line) and numerical solutions (symbols) of the reaction-diffusion model problem at time $t = 1$: (a) u component; (b) v component. The numerical solution is obtained using $S = 16$, $\Delta t = 3.914 \cdot 10^{-4}$, and $N = 512$. The initial condition (black line) is also shown for comparison.

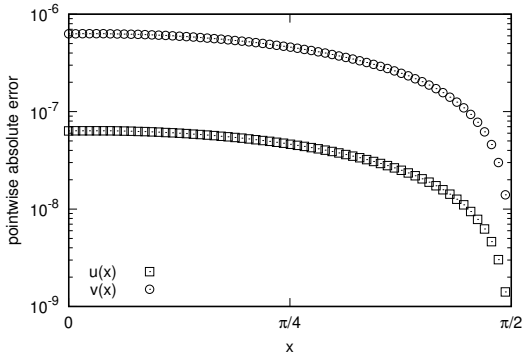

Figure A2. Spatial profiles of the absolute difference between the analytical and numerical solution ($S = 16$, $\Delta t = 3.914 \cdot 10^{-4}$, $N = 512$) of the reaction-diffusion problem at time $t = 1$. Plotted are curves for the u and v components, as indicated.

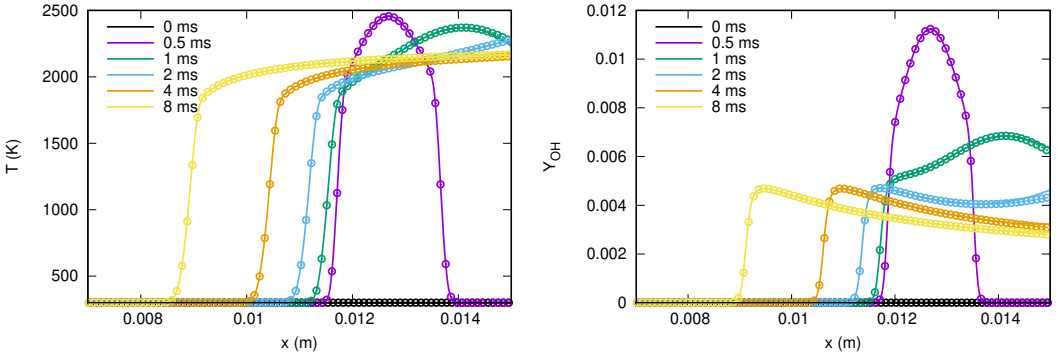

(a) Temperature. (b) OH mass fraction.

Figure A3. Spatial profiles of (a) temperature, and (b) OH mass fraction. Plotted are curves generated at different time instants, as indicated; solid lines are used to depict results obtained using the hybrid scheme, whereas symbols are used to indicate results obtained using RDR Strang splitting. Both the hybrid and split schemes used a grid with 768 nodes equally spaced on a 1.5cm-long domain, a global time step $\Delta t = 500\,\text{ns}$, and $S = 8$ RKC stages.

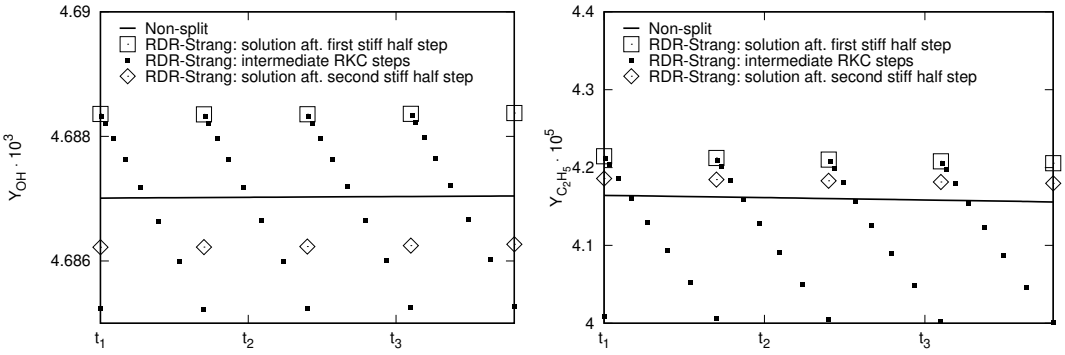

(a) OH mass fraction. (b) C_2H_5 mass fraction.

Figure A4. Evolution of the peak value of (a) OH mass fraction, and (b) C_2H_5 mass fraction, at $t = 20\,\text{ms}$ over the three subsequent time steps. The solid line depicts the intermediate solution after each internal stage of the hybrid non-split method. The open squares and diamonds respectively represent the numerical solution at the end of the first and second stiff integration half steps of the RDR split scheme, whereas the solid squares represent the solution after internal stage of the RKC treatment of diffusion-advection. Both the hybrid and spilt schemes used a grid with 768 nodes equally spaced on a 1.5cm-long domain, a global time step $\Delta t = 400\,\text{ns}$, and $S = 8$ RKC stages.

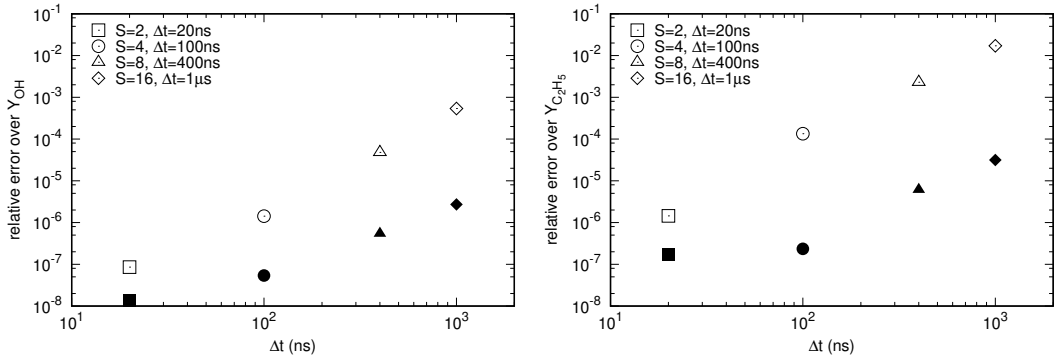

(a) OH mass fraction. (b) C_2H_5 mass fraction.

Figure A5. Relative distance between the reference solution and hybrid solution (solid symbols) and between the reference solution and split solution (open symbols). Results are generated using the predicted OH (left) and C_2H_5 (right) mass fractions at the end of the simulations, for different (Δt,S) pairs, as indicated. In all cases, the solutions were obtained on a grid with 768 nodes equally spaced on a 1.5cm-long domain. The reference solution is computed on the same computational grid, using the hybrid scheme with $S = 2$ and $\Delta t = 1\,\text{ns}$.